Proposal to JLab PAC44 June 6 2016

An isospin dependence study of the ΛN interaction through the high precision spectroscopy of Λ-hypernuclei with electron beam

(update of the conditionally approved C12-15-008)

JLab Hypernuclear Collaboration

Spokespersons:

F. Garibaldi[1], P.E.C. Markowitz[2], S.N. Nakamura[3*], J.Reinhold[2], L. Tang[4,5], G.M. Urciuoli[1]

[1]*Istituto Nazionale di Fisica Nucleare, Sezione di Roma, Gr. Coll. Sanita',Viale Regina Elena 299, Rome, Italy*
[2]*Florida International University, Miami, Florida 33199, USA*
[3]*Department of Physics, Graduate School of Science, Tohoku University, Sendai, 980-8578, Japan*
[4]*Thomas Jefferson National Accelerator Facility, Newport News, Virginia 23606, USA*
[5]*Department of Physics, Hampton University, Hampton, Virginia, 23668, USA*
** Contact person*

JLab Hypernuclear Collaboration

A. Lovato
Argonne National Laboratory

D.J. Millener
Brookhaven National Laboratory

K. Aniol
California State University

T. Horn
Catholic University of America

F. Benmokhtar
Duquesne University

P.E.C. Markowitz (spokesperson), J. Reinhold (spokesperson)
Florida International University

P. Gueye, B.Pandey, L. Tang (spokesperson)
Physics Department, Hampton University

G. De Cataldo, R. De Leo, D. Di Bari, L. Lagamba, E. Nappi
INFN/ Bari

M. Carpinelli, A. Contini, P. Oliva, V. Sipala

INFN/ Cagliari

V. Bellini, M. Bondi, P. Castorina, M. De Napoli, A.S. Italiano, V. Kuznetsov, E. Leonora, F. Mammoliti, N. Randazzo, G. Russo, M. Russo, C.M. Sutera, F. Tortorici
INFN/ Catania

I. Balossino, L. Barion, G. Ciullo, M. Contalbrigo, A. Drago, P. Lenisa, A. Movsisyan, L.L. Pappalardo, F. Spizzo, M. Turisini
INFN/ Ferarra

A. Biselli, D. Hasch, V. Lucherini, M. Mirazita, S. Pisano
INFN/ Frascati

M. Battaglieri, G. Bracco, A. Brunengo, A. Celentano, R. De Vita, E. Fanchini, V. Mathieu, P. Musico, M. Osipenko, L. Perasso, M. Ripani, M.G. Taiuti
INFN/ Genova

R. Perrino
INFN/ Lecce

G. Simi
INFN/ Padova

E. Cisbani, F. De Persio, A. Del Dotto, F. Garibaldi (spokesperson),
F. Meddi, G.M. Urciuoli (spokesperson)
INFN/ Rome

L. Colaneri, A. D'Angelo, L. Lanza, A. Rizzo, I. Zonta
INFN/ Rome Tor Vergata

D. Calvo, A. Filippi, M. Genovese, A.M. Scarfone
INFN/ Torino

T. Takahashi, Y. Sato
Institute for Particle and Nuclear Physics, KEK

T. Holmstrom
Longwood University

S. Gandolfi
Theoretical Division, Los Alamos national Laboratory

J. Pochodzalla, P.Achenbach
Institute fur KernPhysik, Johannes Gutenberg University Mainz

A. Ahmidouch, S. Danagoulian,
North Carolina A&T State University

S.C. Dusa, C. Keppel, S.A. Wood
Thomas Jefferson National Accelerator Facility

D. Lonardoni
National Superconducting Cyclotron Laboratory, Michigan State University and
Theoretical Division, Los Alamos National Laboratory

F.R. Wesselmann
Old Dominion University

T. Gogami
Research Center for Nuclear Physics, Osaka University

E. Hiyama, M. Isaka, Y.Yamamoto
RIKEN

M. Elaasar
Southern University at New Orleans

P. Bydžovský
Nuclear Physics Institute, Řež near Prague

T. Motoba
Laboratory of Physics, Osaka Electro-Communication University

V. M. Rodriguez
Universidad Metropolitana, San Juan, Puerto Rico

G. Aida, M.Fujita, M. Kaneta, H. Kanda, K. Maeda, S. Nagao,
S.N. Nakamura (spokesperson), H. Takeuchi, S. Tomita, Y.Toyama, Y.Muroi
Graduate School of Science, Tohoku University

Y. Fujii
Tohoku Medical and Pharmaceutical University

F. Pederiva
Physics Department, University of Trento and INFN-TIFPA

C. Samanta
Dept. of Physics & Astronomy, Virginia Military Institute

J. Hoskins
College of William and Mary

A. Margaryan
Yerevan Physics Institute, Yerevan, Armenia

D. Androic, M. Furic
Department of Physics, University of Zagreb

T. Petkovic
Faculty of Electrical Engineering and Computing, Department of Applied Physics, University of Zagreb

Abstract

An ambitious and challenging experimental program was started at Jefferson Lab 15 years ago, producing high-resolution hypernuclear spectroscopy via the $(e,e'K^+)$ reaction which is the latest and most accurate reaction spectroscopic technique for hypernuclear study. Data have been taken in both Hall A and Hall C on p-shell and medium-mass targets, providing clear spectra with 0.5~0.8-MeV energy resolution. The $(e,e'K^+)$ reaction spectroscopy of hypernuclei was established at JLab and it is now widely recognized as a powerful tool to study hypernuclei like (K^-,π^-) and (π^+, K^+) reactions. The $(e,e'K^+)$ reaction has advantages in energy resolution over hadronic probes and complements them in being a dominantly spin-flip reaction as opposed to a non-spin flip reaction. The greater strength

observed for the low-lying excited states of $^{12}_{\Lambda}$B relative to the ground state is an example of the advantage sometimes afforded by the spin-flip capability. Gamma-ray spectroscopy, while extremely powerful, is limited to particle-bound states (and thus in light nuclei) and is able to measure level spacing. The (e,e′K^{+}) reaction enables the determination of binding energies with high precision because of the calibration provided by the elementary reaction on hydrogen.

There are growing efforts worldwide in hypernuclear spectroscopy: J-PARC has now re-started hypernuclear physics programs, the decay-pion spectroscopy technique has achieved great success at Mainz and a new exotic hypernucleus was claimed to be found at GSI. Even though plans for various new hypernuclear physics studies exist at different facilities, the precision and accuracy of the mass spectroscopy of the JLab program are unchallengeable, in addition to the clearly known common advantages of electro-production (such as the size of momentum transfer, extra spin transfer from the virtual photon, converting a proton to a Λ for neutron rich hypernuclei *etc.*).

The 6 GeV experiments provided sufficient experience to establish the new program for CEBAF in the 12 GeV era. The outcome of the past activity is the base for building this experimental program in hypernuclear spectroscopy, which will be carried out exploiting techniques that are complementary to the ones adopted by other laboratories.

The JLab hypernuclear collaboration proposed a coherent series of measurements on Λ hypernuclei in a wide mass range of targets to investigate the ΛN interaction and various forms of quantum many-body systems to PAC43. The PAC43 recognized that the isospin dependence study of Λ hypernuclei is currently missing information and it is a key issue to be studied at JLab. The PAC43 conditionally approved the spectroscopy of $^{40}_{\Lambda}$K and $^{48}_{\Lambda}$K as C12-15-008.

This is the updated proposal of C12-15-008 focusing on the isospin dependence of the ΛN interaction, following requirements of PAC43 for a full approval of the program. It should be noted that the new optimized experimental design does not only widen and deepen the physics investigation range and topics but also dramatically improves on the data quality and production efficiency, maximizing the physics output.

The recent observation of neutron stars with masses accurately measured to be larger than two solar mass posed a challenge to our present knowledge of the interaction among baryons in high-density matter. In the interior of a neutron star which is highly asymmetric nuclear matter, nucleons reach densities overcoming the one of nuclei by several times. In these conditions, the appearance of strangeness, in the form of hyperons, is energetically

favored, since it helps to reduce the Fermi energy of nucleons. However, present theoretical models typically predict that this energy reduction (and the consequent "softening" of the equation of state) would lead to neutron stars with a mass smaller than $1.5M_{\odot}$. This is the so-called "hyperon puzzle", that is currently one of the unsolved key issues in the physics of compact stars.

Relating the experimental findings on hypernuclei to the equation of state of dense matter is a highly non-trivial task. The key issue is an accurate determination of the hyperon-nucleon interaction. There is a general consensus that such interaction should be more repulsive than what supposed so far, and hypernuclear spectroscopy data are necessary to constrain it. However, hypernuclei and matter in the interior of neutron stars differ for the excess of neutrons present. In the core of neutron star matter is made by more than 90% of neutrons. This requires that the effects of asymmetry (that one can translates into an isospin dependence of the hyperon-nucleon force) need to be investigated at a very high level of accuracy in order to make reliable prediction on the neutron star structure and dynamics. The proposed experiment exactly addresses this fundamental issue.

1. Introduction

Nuclear physics has the major goal of understanding the nature of many-body system whose dynamics is dictated by the strong interaction. In the universe, there is a hierachy of three such systems: 1) baryons/mesons, the bound system of quarks, 2) nuclei, the self-bound system of baryons and 3) neutron stars, isospin-asymmetric nuclear matter bound by gravitational effects. The size scale of 1) and 2) is femtometers and that of 3) is ~10 km. Though they differ by 10^{19} order of magnitudes, the interactions governing their structure and properties are the same. The strong interaction in the low energy region where the QCD is not perturbative has been investigated in the framework of baryon potential models. The construction of NN potentials has taken advantage upon the availability of a substantial number of scattering data. High-precision potential models fit all these data with extreme accuracy. However, when only two-body forces are accounted for, light nuclei turn out to be under-bound and the saturation properties of infinite isospin-symmetric nuclear matter are not correctly reproduced. It indicates the need for a three-body interaction. The same theoretical framework could be extended to the strange sector. Though the strange quark is heavier than the u and d quarks, it is still lighter than the QCD cut-off (~1 GeV) unlike the heavy quarks (c, t, b). Hence, the strange quark can be treated in the framework of the flavor SU(3) symmetry which is a natural extension of the isospin symmetry for ordinary nucleons. To devise a unified description of the baryonic interaction within the flavor SU(3) basis, one must then quantitatively understand the hyperon-nucleon (YN) and the hyperon-hyperon (YY) interactions. Spectroscopic investigation of Λ-hypernuclei, nuclear many-body systems containing one Λ particle, provides a unique and, currently, the only practical tool to study the ΛN interaction. Direct ΛN scattering experiments are technically very difficult.

While several models of YN forces were proposed in the past, recent observation of neutron stars with masses of $2M_{\odot}$ (two solar mass) poses several important questions. There is a very simple argument to justify the appearance of strange degrees of freedom in the inner core of a neutron star. In the pure neutron matter case, whenever the chemical potential becomes sufficiently large to match the chemical potential of a hyperon in the same matter, the hyperon becomes stable since it is a distinguishable particle, and creates its own Fermi sea, thereby lowering the kinetic energy of the system. This results in a

so-called "softening" of the equation of state, due to a decrease of the Fermi pressure. In turn, a soft equation of state predicts a lower sustainable mass for a neutron star. So far, existing YN interactions typically predict a maximum mass no larger than $1.5M_{\odot}$, in strong contrast with the astrophysical observations (the "hyperon puzzle"). The key for solving this apparent contradiction is a more repulsive YN interaction, which increases the hyperon chemical potential, moving the onset of hyperons at higher densities. Most models nowadays agree on this aspect, but additional constraints are needed and they can only be inferred from accurate spectroscopic data of hypernuclei

The relation between hypernuclei and matter inside a neutron star is not straightforward. In particular, one has to remember that neutron stars are indeed 90% made up by neutrons. Hypernuclei, instead, have a neutron fraction not exceeding 60%. It is clear that the effect of asymmetry of the nuclear medium on the hyperon chemical potential (which can be for instance translated into an isospin dependence of YNN interaction) cannot be effectively constrained from the existing hypernuclear data, unless very accurate measurements on asymmetric hypernuclei are performed. Tiny changes in the binding energy, and consequently on the determination of the YN/YNN force, can have dramatic consequences on the EoS of matter at supra-saturation conditions.

Another interesting aspect of the isospin dependence of the YN interaction is the charge symmetry breaking (CSB). Recently decay-pion spectroscopy of electro-produced ${}^{4}_{\Lambda}$H, which was originally proposed at JLab [LER13], was successfully carried out at Mainz [ESS15] and the excitation energy of ${}^{4}_{\Lambda}$He 1^{+} state was also successfully measured by the gamma-spectroscopy at J-PARC [TOY15]. These new experimental data strongly support the fact that the A=4 hypernuclear iso-doublet has a large CSB for the ground states (0^{+}) and small CSB for the 1^{+} states. Although the origin of such a large CSB is not fully understood, it is clear that the discussion based on 2-body YN/NN interaction only does not suffice and that the inclusion of ΛN-ΣN coupling and 3-body force is essential. For heavier and neutron richer hypernuclear systems, such ΛN-ΣN coupling and 3-body force become more important, implying that the behavior of Λ in symmetric nuclear matter and neutron-rich environments would be quite different.

The accuracy of existing hypernuclear data is not adequate to the features of the baryonic

force models needed to properly address the hyperon puzzle, and thus higher precision data are necessary. It should be noted that a systematic study of $A \leq 209$ Λ hypernuclei with ~1 MeV accuracy has already been carried out, but no experimental efforts have been made so far to systematically study the various aspects of the isospin dependence of the ΛN interaction.

We propose to measure Λ binding energies of $^{40}_{\Lambda}$K and $^{48}_{\Lambda}$K via ^{40,48}Ca (e,e'K^{+})$^{40,48}_{\Lambda}$K reactions. **Precise hypernuclear spectroscopy on medium to heavy hypernuclei, crucially important to obtain a reliable interaction which can be used to calculate EOS of the neutron stars, is only feasible using the CEBAF electron beam** and cannot be performed at other facilities due to equipment and beam quality constraints.

References

[LER07] JLab Hypernuclear Collaboration, PR12-13-002 submitted to JLab PAC40.

[ESS15] A.Esser, S,Nagao, F.Schulz et al., Phys, Rev. Lett. 114 (2015) 232501.

[TOY15] T.O.Yamamoto et al., Phys, Rev. Lett. 115 (2015) 222501.

2. Proposed experiment

The proposed experiment is the update of the conditionally approved experiment, C12-15-008. The PAC43 recognized the importance of the study of the isospin dependence of the three-body hyperon-nucleon force as a fundamental ingredient for the possible solution of the hyperon puzzle, a very actual issue in nuclear astrophysics raised after the observation of two solar masses neutron stars. The PAC43 suggested the proponents to re-design the experiment with a priority on the isospin dependence study. We, JLab Hypernuclear Collaboration, have updated the proposal focusing on spectroscopy of $^{40}_{\Lambda}$K and $^{48}_{\Lambda}$K through the ^{40}Ca(e,e′K^{+})$^{40}_{\Lambda}$K and ^{48}Ca(e,e′K^{+})$^{48}_{\Lambda}$K reactions following the PAC43 recommendations.

The technique of (e,e′K^{+}) hypernuclear spectroscopy is currently the only method that can measure the absolute hypernuclear binding energy centroids for ground and excited states with an unprecedented accuracy of <100 keV. It should be noted that reaction spectroscopy such as (e,e′K^{+}) hypernuclear spectroscopy provides information on the cross section as well as the binding energy information. The production information is complementary to the information obtained by decay product studies such as gamma and decay-pion spectroscopies.

In this section, the physics justification of the measurement will be detailed.

2.1 Neutron Stars and the Hyperon Puzzle

Neutron stars (NS) are the most compact and dense stars in the universe, with typical masses $M \sim 1.4\, M_{\odot}$ and radii R~10 km. Their central densities can be several times larger than the nuclear saturation density, $\rho_0 = 0.16$ fm^{-3}. Since the Fermi energy of fermions at such densities is in excess of tens of MeV, thermal effects have little influence on the structure of NS. Therefore they exhibit the properties of cold matter at extremely high densities, very far from being realized in present terrestrial experiments. In the era of multi-messenger astronomical observations, NS offers a unique opportunity to test a broad class of theories, from nuclear physics to general relativity, including the recent observation of gravitational waves.

From the surface to the interior of a NS, stellar matter undergoes a number of transitions. From electron and neutron-rich ions in the outer envelopes, the composition is believed to change into a degenerated gas of neutrons, protons, electrons and muons in the outer core.

At densities larger than ~$2\rho_0$ new hadronic degrees of freedom or exotic phases are likely to appear. Fig.2-1 shows the chemical potentials and concentrations of stellar constituents in beta-stable hyperonic matter as a function of baryon density, obtained from a recent theoretical calculation employing modern baryonic potentials [Bom16].

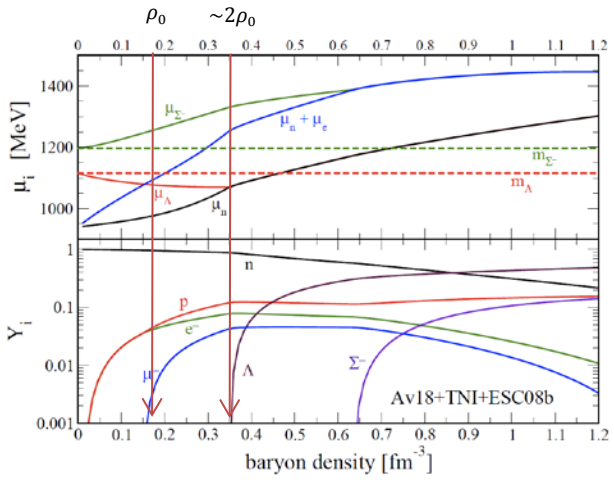

Figure 2-1: Chemical potentials μ, and concentrations Y of the stellar constituents in hyperonic matter as a function of the baryon density [Bom16].

The first theoretical indication for the appearance of hyperons in the core of a NS was already advocated in 1960 [AMB60]. In the degenerate dense matter forming the inner core of a NS, Pauli blocking would prevent hyperons from decaying by limiting the phase space available to nucleons. When the nucleon chemical potential is large enough, the conversion of nucleons into hyperons becomes energetically favorable. This results in a reduction of the Fermi pressure exerted by the baryons and a softening of the equation of state (EOS). As a consequence, the maximum mass determined by the equilibrium condition between gravitational and nuclear forces is reduced. The value of about $1.5M_{\odot}$ for the maximum mass of a NS, inferred from neutron star mass determinations [THO99], was considered the canonical limit, and it was compatible with most EOS of matter containing strangeness. However, the recent measurements of the large mass values of the millisecond pulsars J1614-2230 (1.97(4)$M_{\odot}$) [DEM10] and PSR J0348+0432 (2.01(4)$M_{\odot}$) [ANT13] require a much stiffer equation of state.

This seems to contradict the appearance of strange baryons in high-density matter given what is known at present about the hyperon-nucleon interaction. This apparent inconsistency between NS mass observations and theoretical calculations is a long-standing problem known as "**hyperon puzzle**". Its solution requires better understanding of the YN interaction in a wide range of systems from light to medium and heavy hypernuclei as well as more accurate theoretical calculation frameworks.

Currently there is no general agreement (even qualitative) among the predicted results for the EOS and the maximum mass of NS including hyperons. This has to be ascribed to the combination of an incomplete knowledge of the forces governing the system (in the hypernuclear case both two- and three-body forces), and to the concurrent use of approximated theoretical many-body techniques. Some classes of methods extended to the hyperonic sector predict the appearance of hyperons at around 2-3ρ_0, and a strong softening of EOS, implying a sizable reduction of the maximum mass [VID11, HJS11, MAS12]. On the other hand, other approaches suggest much weaker effects arising from the presence of strange baryons in the core of the star [BED12,WEI12,MIY13,LOP14].

The large body of available nucleon-nucleon scattering data allows one to derive satisfactory models of two-body nuclear forces, either purely phenomenological [WIR95] or built on the basis of an effective field theory [MAC96, EPE05, EKS13, GEZ13]. In the hyperon-nucleon sector, few scattering data are available, although a ΣN scattering experiment is currently in preparation at J-PARC [MIW11], and no scattering data exist in the hyperon-hyperon sector. The main reasons of this lack of information lie in the instability of hyperons in the vacuum, and the impossibility of collecting hyperon-neutron and hyperon-hyperon scattering data. This implies that realistic hypernuclear interaction models must also rely on information extracted from the binding energies of hypernuclei.

In the non-strange nuclear sector the binding energies of light nuclei have been used to constrain three-nucleon potential models. However, the most accurate phenomenological three-body force (Illinois 7 [PIE08]), while providing a satisfactory description of the spectrum of light nuclei up to ^{12}C [PIE08] yields to a pathological EOS for pure neutron matter (PNM) [MAR13]. On the other hand, when additional information on the three-nucleon interaction is inferred from saturation properties of symmetric nuclear matter

(Urbana IX force [PUD95]), the resulting PNM EOS turns out to be stiff enough to be compatible with astrophysical observations [GAN12].

Recent analysis of ^{16}O-^{16}O scattering data shows that the established meson exchange potential model (Nijmegen ESC08c [NAG14]) cannot reproduce the cross section at large scattering angles and inclusion of 3-body/4-body repulsive forces solves the problem [FUR09].

Thus, there is a general indication that 3-body/4-body repulsive forces become quite significant at high density, but they cannot be constrained from light systems. In a similar fashion, the binding energies of light hypernuclei do not suffice in constraining hypernuclear interactions. Additional information must necessarily be inferred from the properties of medium and heavy hypernuclei in order to extrapolate to the infinite-mass limit for discussion of highly massive asymmetric nuclear matter such as neutron stars and strange hadronic matters ($n_u \sim n_d \sim n_s$).

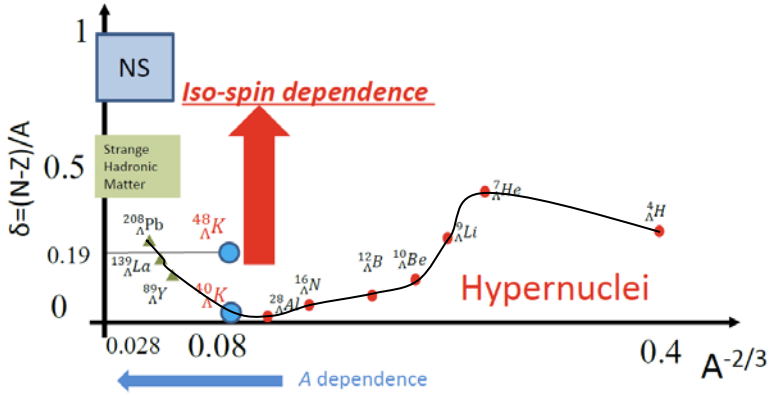

Figure 2-2: Schematic description of the behavior of the asymmetry parameter δ as a function of $A^{-2/3}$. The regions corresponding to NS, strange hadronic matters and hypernuclei are highlighted. The blue closed circles represent the case for $^{40}_{\Lambda}$K (δ=0.025) and $^{48}_{\Lambda}$K (δ=0.188).

Figure 2-2 shows the dependence of the asymmetry parameter $\delta=(N-Z)/A$ as a function of $A^{-2/3}$ for strange systems. The regions corresponding to neutron stars ($\delta = 0.9, A\sim\infty$), strange hadronic matter ($\delta = 0.5, A\sim\infty$) and hypernuclei are highlighted. Precise data of light neutron rich hypernuclei were recently obtained at JLab. Though they play an important role to extract information about baryonic interactions, they are too light to discuss the properties of strange nuclear matter. Heavier hypernuclei have been studied with pion beams but the achieved precision is not enough to extract detailed information about the 3-body hyperon-nucleon force. Furthermore, spectroscopic studies of hypernuclei

have been carried out with stable target nuclei along the Heisenberg valley and there is little freedom to simultaneously control isospins and masses for heavy hypernuclei. The proposed experiment will study the two medium-heavy hypernuclear isotopes $^{40}_{\Lambda}$K and $^{48}_{\Lambda}$K, which show very different isospin asymmtry (δ=0.025 and 0.118, respectively), in order to extract isospin dependence of the 3-body ΛNN force. Such information is essential to extrapolate the hyperon behavior to the infinite limit and thus to reliably predict neutron star properties.

2.2 Theoretical models

The structure of Λ hypernuclei is generally studied by employing the weak-coupling approximation that assumes the wave function of a Λ hypernucleus to be decomposed into a core nucleus and a Λ hyperon. In this picture, the hypernuclear Hamiltonian consists of the Hamiltonian for the core-nucleus, the Λ kinetic energy and the sum of ΛN interaction terms that can be derived with various theoretical frameworks.

From the analysis of hypernuclear binding energies and the limited available YN scattering data, different baryon-baryon interaction models have been formulated, based on meson exchange picture such as Nijmegen ESC08c [NAG14,NAG15] or derived from chiral effective field theory(CEFT) [HAI13]. In order to analyze structure of heavier hypernuclei, the hypernuclear effective interactions have been derived from the free ΛN force by various calculation techniques such as G-matrix methods.

As already recognized in the non-strange sector by the study of ^{16}O-^{16}O scattering data [FUR09], the ESC08c model needs to be supported by a 3/4-body repulsive force (MPa) that can be universally extended to the strange sector.

On the other hand, CEFT established a prescription to extend the interaction model to include many-body forces. Performed next-to-leading order (NLO) calculations already included some components of the 3-body force (the ones that can be reduced to 2-body terms), but next-to-next-to-leading order (NNLO) calculations are necessary for the inclusion of a genuine 3-body interaction, and more experimental inputs are required to constraint the low-energy constants.

Recently, the auxiliary field diffusion Monte Carlo (AFDMC) technique for strange systems has made substantial progresses. By using this microscopic ab-initio approach, an accurate analysis of the Λ separation energy of light- and medium-heavy hypernuclei has been carried out [LON14, PED15] using a phenomenological interaction [BOD84, USM95, IMR14] in which the two-body potential has been fitted on the existing Λp scattering data. As shown in Fig.2-3(a), when only the two-body ΛN force is considered (red curve), the calculated hyperon separation energies tend to disagree with the experimental data (green curve) as the density increases. The inclusion of the three-body ΛNN force in this scheme leads to a satisfactory description of the hyperon separation energies in a wide mass range and for the Λ occupying different single particle state orbitals (s, p and d wave), as shown in Figs. 2-3(b).

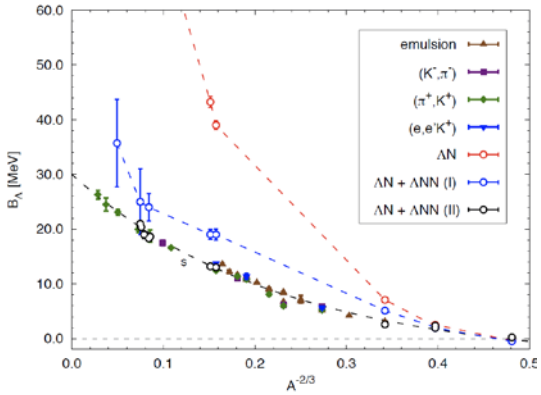

(a) Experimental B_Λ values in s wave and AFDMC calculation results with 2-body ΛN interaction alone, and two different parametrizations of the 3-body YN interaction (updated from [LOD14]).

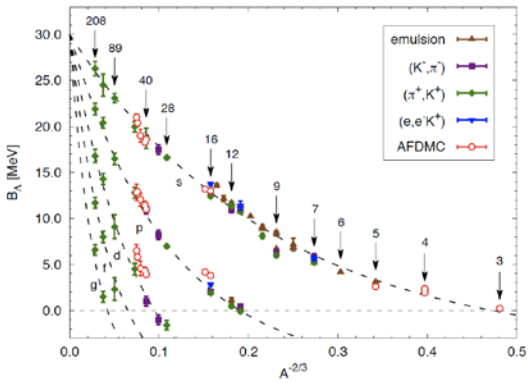

(b) Experimental results for Λ in s, p, d, f and g waves. Red open circles are the AFDMC results obtained including the most recent 2-body plus 3-body hyperon-nucleon phenomenological interaction model (updated from [PED15]).

Figure 2-3: Λ separation energies as a function of $A^{-2/3}$. Predicted results for $^{40}_{\Lambda}$K and $^{48}_{\Lambda}$K are also included.

However, these potential models predicting relatively small differences in the Λ separation energies of hypernuclei give dramatically different results as for the properties of the infinite medium [LON15]. The resulting EOS spans the whole regime extending from the appearance of a substantial fraction of hyperons at $\sim 2\rho_0 \simeq 0.32$ fm^{-3} to the absence of Λ particles in the entire density range of the star, as shown in Fig. 2-4(a). This has a sizable effect on the predicted NS structure, Fig. 2-4(b).

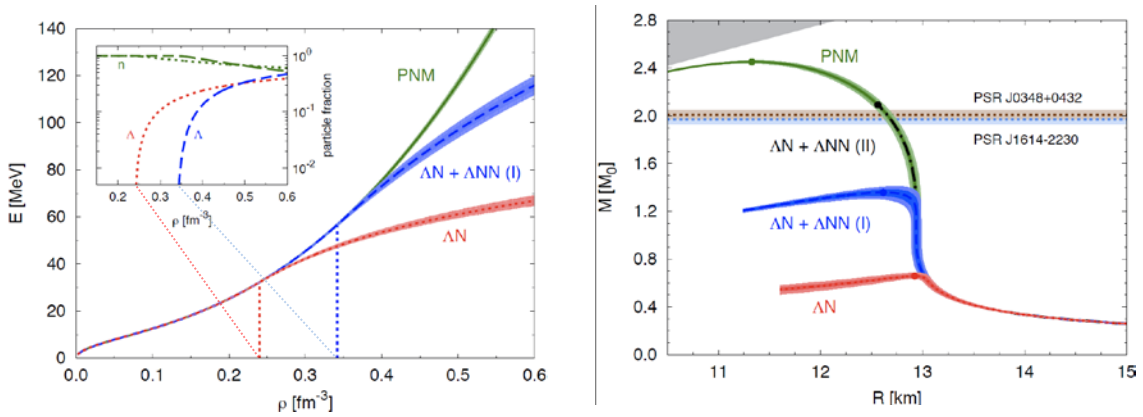

(a) Equations of state. The vertical dotted lines indicate the Λ threshold densities. In the inset, neutron and Λ fractions corresponds to the two hyper-neutron matter EOSs.

(b) Mass-radius relations given by AFDMC. Closed circles represent the predicted maximum masses. Horizontal bands at $2M_{\odot}$ are the observed masses of the heavy neutron stars [DEM10, ANT13].

Figure 2-4: EOS and neutron star mass-radius relations calculated by AFDMC [LON15].

Other techniques such as G-matrix or AMD calculations employing multi-baryon interactions, for instance the the ESC08c+MPa potential, are able to reprocude B_{Λ} of a wide range of hypernuclei with accuracy of <1 MeV and similar result for EOS of neutron stars which can support 2 solar mass was obtained [YAM14, ISA16].

Although these calculations are based on different theoretical techniques and different baryonic potential models, they all predict in a similar tendency of large 3-body repulsive forces at high density, suggesting a possibility to make the EOS of hyper-nuclear matter hard enough to support 2 solar mass neutron stars.

However, while 2-body baryonic force models based on different theoretical frameworks are reasonably accurate, detailed information on the 3-body hyperon-nucleon interaction is still missing. In particular very little is known on the isospin dependence of such multi-baryon forces, which plays a crucial role in the determination of the structure of neutron stars. This lack of knowledge is to be attributed to a poor experimental information for medium-heavy neutron-rich hypernuclei, which are the key to infer properties of the infinite hyper-nuclear matter. Therefore, in order to properly assess the role of hyperons in NSs and reconcile theoretical predictions with astrophysical observations, *i.e.* solve the hyperon puzzle, precise experimental investigation on medium-heavy neutron-rich targets is of paramount importance and only JLab can provide such an accurate experimental data.

2.3 Spectroscopy of $^{40}_{\Lambda}$K and $^{48}_{\Lambda}$K hypernuclei

The region of medium-mass hypernuclei is particularly interesting. Systems with $A \leq 50$ are the most similar to the infinite medium for which ab-initio many-body calculations are feasible. However, present experimental information in the mass region $40 \leq A \leq 50$ relies uniquely on the data measured by the (π^+, K^+) reaction. The resolution as well as absolute energy scale calibration of the (π^+, K^+) data are not satisfactory. The only two hypernuclei for which experimental data exist are $^{40}_{\Lambda}$Ca [PIL91] and $^{51}_{\Lambda}$V [HOT01], the former plagued by very low statistics (Fig. 2-5).

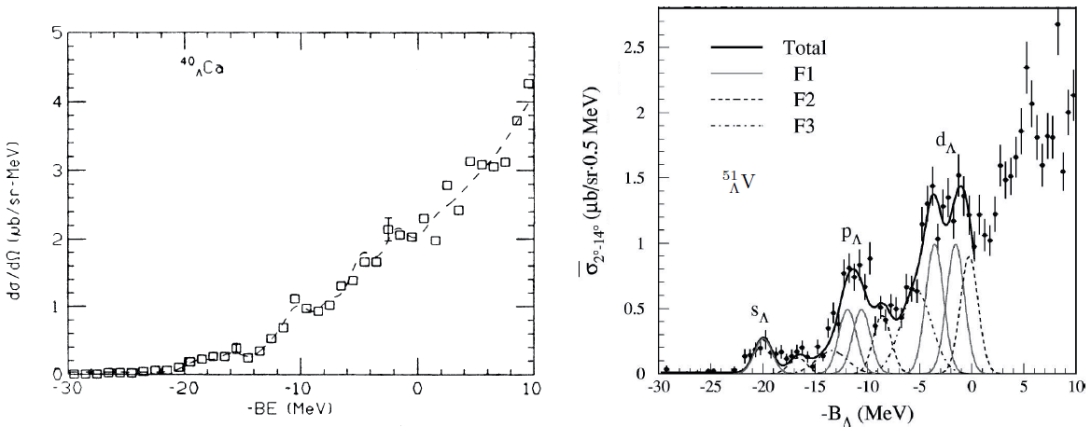

Figure 2-5: $^{40}_{\Lambda}$Ca [PIL91] and $^{51}_{\Lambda}$V [HOT01] spectra obtained by the (π,K) reaction.

Hence, new accurate (e,e'K^+) measurements of the Λ separation energies in the regions A~40 and A~50 are necessary to constrain the behavior of hyperon-nucleon interactions at densities relevant for neutron star. It should be noted that recent results of hypernuclear spectroscopy at JLab reveal that all (π^+, K^+) data, which used the $^{12}_{\Lambda}$C emulsion result as a reference, manifest a systematic shift of B_Λ by 0.54 MeV [GOG16, EUR16]. By using the elementary reaction on hydrogen, the (e ,e′K^+) spectroscopic experiment can calibrate its energy scale without any reference from other experiments. It offers the JLab the opportunity to establish a new standard in precision hypernuclear spectroscopy on medium-heavy targets.

As recognized by JLab PAC43, precise measurements of B_Λ in ^{40}Ca(e,e′K^+)$^{40}_{\Lambda}$K and ^{48}Ca(e,e′K^+)$^{48}_{\Lambda}$K will provide accurate and reliable experimental information in the mass

region of interest $40 \leq A \leq 50$, allowing to assess the isospin dependence of the hyperon-nucleon force.

The original parametrization of the ΛNN potential used in quantum Monte Carlo calculations does not depend on whether the two nucleons are in isospin singlet (T=0) or isospin triplet (T=1) state. For symmetric hypernuclei the Pauli principle suppresses any strong contribution from the Λnn or Λpp channels. On the other hand, in neutron matter or in matter at beta-equilibrium the contribution of the isospin triplet channel will become quite relevant. Introducing a control parameter C_T in order to gauge the strength and the sign of the isospin triplet component, it has been shown [PED15] that AFDMC results are sensitive to the isospin asymmetry only in the medium-mass region (Fig. 2-6). For light hypernuclei the results are compatible with the measured B_Λ in the range -1< C_T <1.5, which implies that the isospin asymmetry contribution is essentially undetermined. The results for heavier asymmetric hypernuclei are instead more sensitive to the variation of C_T, in particular for $A \sim 50$.

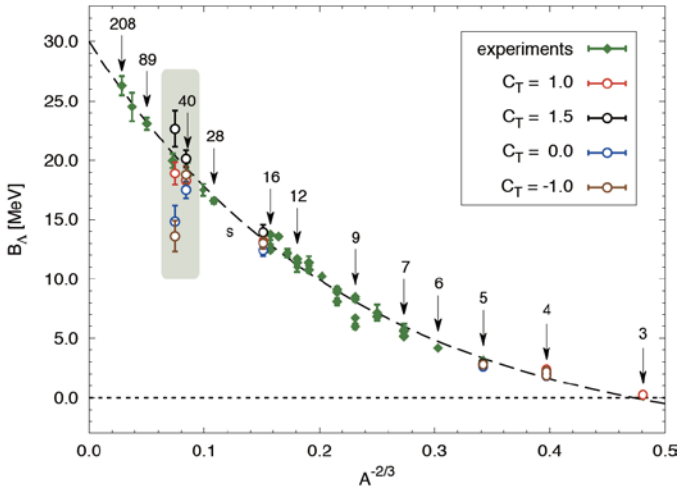

Figure 2-6: Λ separation energies as a function of $A^{-2/3}$ with various values of the control parameter C_T. C_T =1 recovers the original 3-body hyperon-nucleon force. The shaded region represents the zone of interest for the presenting proposal.

However, current experimental information in this mass region cannot provide ANY information on the possible isospin dependence of hypernuclear forces. Fig.2-7 shows the Λ separation energy for 40<A<50 as a function of the neutron number N. Open circles refer to the AFDMC results for different proton number (Z=19, 20), closed diamonds are the original (π^+,K^+) experimental data. Due to the large experimental error bars, $^{40}_{\Lambda}$Ca and $^{51}_{\Lambda}$V

are indistinguishable in this plot and the two B_Λ's do not make meaningful difference. On the other hand, the precision achieved in quantum Monte Carlo calculations, that can be still systematically improved, is already good enough to distinguish systems with different neutron number like ${}^{40}_{\Lambda}$K and ${}^{48}_{\Lambda}$K, making the isospin dependence of the hyperon-nucleon interaction an accessible property.

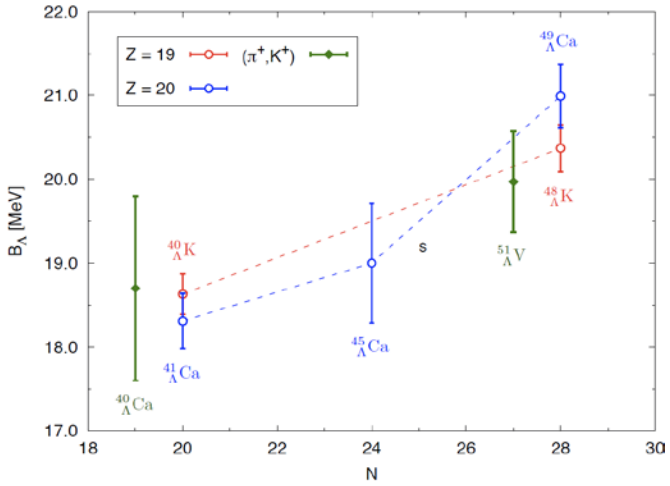

Figure 2-7: Λ binding energies separation energy in s-wave as a function of the neutron number N. Empty circles refer to the AFDMC results for different proton number (red for Z=19, blue for Z=20). Closed green diamonds are the original (π^+,K^+) experimental data.

Thus, precise (e, e′ K^+) measurements of the Λ separation energies of ^{40}Ca(e ,e′K^+)${}^{40}_{\Lambda}$K and , ^{48}Ca(e,e′K^+)${}^{48}_{\Lambda}$K will provide strong constraints on the three-body hyperon-nucleon interaction.

Establishing the isospin dependence of the ΛNN force is of major interest. In a quite asymmetric nucleus as ${}^{48}_{\Lambda}$K, where $\delta = (N-Z)/A \simeq 0.19$, the C_T dependence of B_Λ is appreciable due to the larger contribution arising from Λnn triplets. In NS matter the asymmetry parameter is $\delta \simeq 0.9$, and thus the role of the isospin asymmetry is crucial in the determination of the NS structure.

Fig. 2-8 shows the calculated B_Λ of ${}^{40}_{\Lambda}$K and ${}^{48}_{\Lambda}$K as a function of C_T. It shows that ${}^{40}_{\Lambda}$K has little C_T dependence and it can provide good reference for ${}^{48}_{\Lambda}$K which has large C_T dependence. Though further detailed theoretical studies are necessary, the gradient of C_T-B_Λ curve indicates that the proposed experimental accuracy of 100 keV for $B_\Lambda({}^{48}_{\Lambda}\mathrm{K})$

corresponds to 0.02 for $C_{T.}$ Assuming C_T is about 1.0 which is the original ΛNN potential parametrization, the proposed experiment can determine C_T with a precision of 2%.

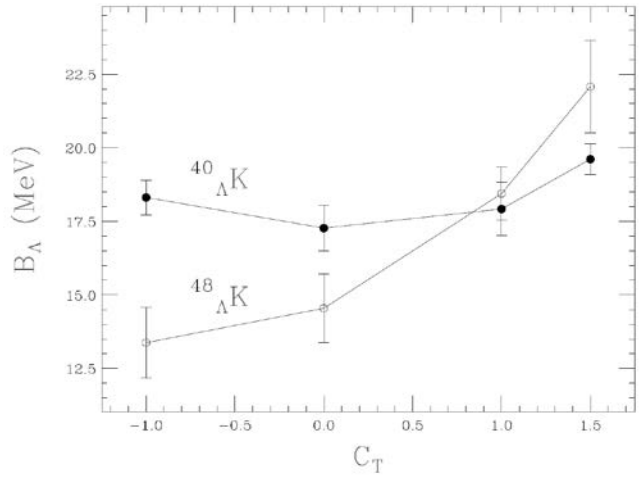

Figure 2-8: Λ separation energies calculated by AFDMC for $^{40}_{\Lambda}$K and $^{48}_{\Lambda}$K as a function of C_T.

References

[BOM16] I.Bombaci, ArXiv:1601.05339; to be published as HYP2015 Proceedings.

[AMB60] V. A. Ambartsumyan and G. S. Saakyan, Sov. Astron. AJ 4, 187 (1960).

[THO99] S. E. Thorsett and D. Chakrabarty, Astrophys. J. 512, 288 (1999).

[DEM10] P. B. Demorest, *et al.*, Nature 467, 1081 (2010).

[ANT13] J. Antoniadis, *et al.*, Science 340, 1233232 (2013).

[VID11] I. Vidana, D. Logoteta, C. Providencia, A. Polls, and I. Bombaci, Europhys. Lett. 94, 11002 (2011).

[HJS11]H.-J. Schulze and T. Rijken, Phys. Rev. C 84, 035801 (2011).

[MAS12] E. Massot, J. Margueron, and G. Chanfray, Europhys. Lett. 97, 39002 (2012).

[BED12] I. Bednarek, *et al.*, Astron. Astrophys. 543, A157 (2012).

[WEI12] S. Weissenborn, D. Chatterjee, and J. Schaffner-Bielich, Phys. Rev. C 85, 065802 (2012);

[MIY13] T. Miyatsu, M.-Ki Cheoun, and K. Saito, Phys. Rev. C 88, 015802 (2013);

[LOP14] L. L. Lopes, and D. P. Menezes, Phys. Rev. C 89, 025805 (2014).

[WIR95] R. B. Wiringa, V. G. J. Stoks, and R. Schiavilla, Phys. Rev. C 51, 38 (1995); R. B. Wiringa and S. C. Pieper, Phys. Rev. Lett. 89, 18 (2002).

[MAC96] R. Machleidt, F. Sammarruca, and Y. Song, Phys. Rev. C 53, R1483 (1996).

[EPE05] E. Epelbaum, W. Glockle, and Ulf-G. Meissner, Nucl. Phys. A 747, 0375 (2005).

[EKS13] A. Ekstrom et al., Phys. Rev. Lett. 110, 192502 (2013).

[GEZ13] A. Gezerlis et al., Phys. Rev. Lett. 111, 032501 (2013).

[MIW11] K. Miwa *et al.* , J-PARC E40 experiment.

[PIE08] S. C. Pieper, AIP Conf. Proc. 1011, 143 (2008); Nuovo Cimento Rivista Serie 31, 709 (2008).

[MAR13] P. Maris, J. P. Vary, S. Gandolfi, J. Carlson, and S. C. Pieper, Phys. Rev. C 87, 054318 (2013).

[PUD95] B. S. Pudliner, V. R. Pandharipande, J, Carlson, R. B. Wiringa, Phys. Rev. Lett. 74, 4396 (1995).

[GAN12] S. Gandolfi, J. Carlson, and S. Reddy, Phys. Rev. C 85, 032801 (2012); S. Gandolfi, J. Carlson, S. Reddy, A. W. Steiner, and R. B. Wiringa, Eur. Phys. J. A 50, 10 (2014).

[NAG14] MM.Nagels, Th.A.Rijen, Y.Yamamoto, arXiv:1408.4825.

[FUR09] T. Furumoto, Y. Sakuragi, Y. Yamamoto, Phys. Rev. C 79 (2009) 0011601(R).

[NAG15] MM.Nagels, Th.A.Rijen, Y.Yamamoto, arXiv:1501.06636.

[HAI13] J.Haidenbauer et al., Nucl. Phys. A 915 (2013) 24.

[LON14] D. Lonardoni, F. Pederiva, and S. Gandolfi, Phys. Rev. C 89, 014314 (2014).

[PED15] F. Pederiva, F. Catalano, D. Lonardoni, A. Lovato and S. Gandolfi, arXiv:1506.04042.

[BOD84] A. R. Bodmer, Q. N. Usmani, and J. Carlson, Phys. Rev. C 29, 684 (1984); A. R. Bodmer and Q. N. Usmani, Phys. Rev. C 31, 1400 (1985).; A. R. Bodmer and Q. N. Usmani, Nucl. Phys. A 477, 621 (1988).

[USM95] A. A. Usmani, S. C. Pieper, and Q. N. Usmani, Phys. Rev. C 51, 2347 (1995); A. A. Usmani, Phys. Rev. C 52, 1773 (1995); Q. N. Usmani and A. R. Bodmer, Phys. Rev. C 60, 055215 (1999); A. A. Usmani and F. C. Khanna, J. Phys. G 35, 025105 (2008).

[IMR14] M. Imran, A. A. Usmani, M. Ikram, Z. Hasan, and F. C. Khanna, J. Phys. G 41, 065101 (2014).

[LON15] D. Lonardoni, A. Lovato, S. Gandolfi, and F. Pederiva, Phys. Rev. Lett. 114, 092301 (2015).

[YAM14] Y. Yamamoto, T. Furumoto, N. Yasutake and Th.A. Rijken, Phys. Rev. C 90 (2014) 045805.

[ISA16] M.Isaka, Y.Yamamoto and Th.A.Rijken, presentation at JLab Hypernuclear workshop (2016).

[PIL91] P. Pile *et al.* , Phys. Rev. Lett. **66** (1991) 2585.

[HOT01] H. Hotchi, *et al.* Phys. Rev. C 64, 044302 (2001).

[GOG16] T.Gogami et al., Phys. Rev. C 93, 034314 (2016).

[EUR16] EurekAlert! "New spectroscopy of $^{10}_{\Lambda}$Be hypernucleus redfines the reference data of Lambda hypernuclei", http://www.eurekalert.org/pub_releases/2016-04/tu-nso040616.php

3. Experimental Setup

3.1 Experimental configuration

The proposed experiment is to obtain high precision mass spectroscopy of hypernuclei produced by the (e,e′K^+) reaction and will employ a configuration including a pair of room temperature Septum magnets, the high resolution HRS (Hall A) and the large solid-angle HKS spectrometers, as schematically illustrated in Fig. 3-1.

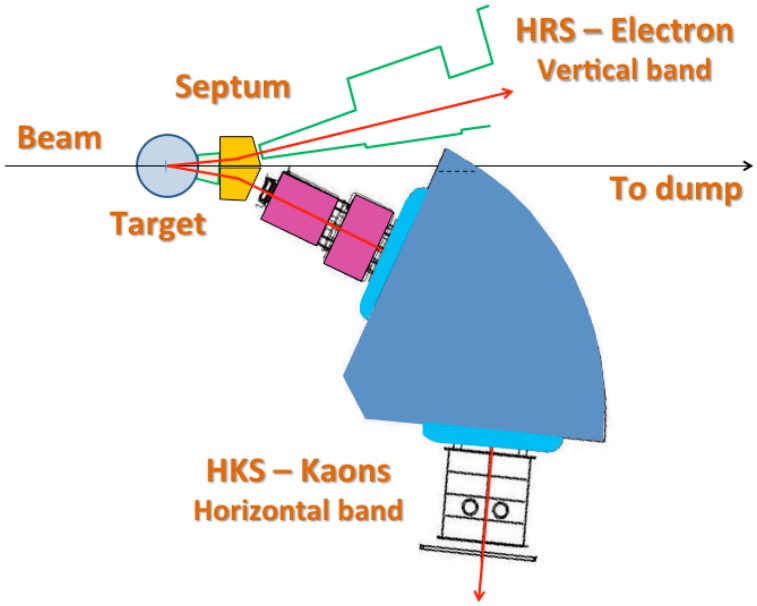

Figure 3-1: Schematic illustration of the experimental layout. A pair of Septum magnets will be used to separate the scattered electrons (analyzed by HRS) and the reaction kaons (analyzed by HKS). All particles at near zero degrees will be sent to the dump.

This pair of Septum magnets will be used to separate the scattered electrons and electro-produced kaons at small forward angles to sufficiently large spectrometer angles, while allowing the post-beam to be directly transported to the dump. It also minimizes the chance for the high rate backgrounds (electrons and positrons) at near zero degrees to enter either of the two spectrometers. The collaboration has demonstrated the technique successful in avoiding the background from e′ and K^+ accidental coincidences by maintaining sufficiently low singles rates at each of the two spectrometers under high luminosity conditions.

One of the Hall A HRS spectrometer will be used to detect and analyze the scattered electrons with a momentum resolution of ~10^{-4} (FWHM) that is crucial to the overall energy resolution for the experiment. With the central scattering plane is defined in the horizontal plane, the vertical bending of HRS provides the important target "Z" vertex reconstruction that will minimize the target "Z" dependence in the optics of the spectrometer system. This is another important feature needed to achieve the ultimate resolution with the extended targets. This is also an important reason for proposing this experiment to run in Hall A.

The HKS spectrometer that was successfully used in the previous Hall C experiments will be used as the kaon spectrometer. It features both a momentum resolution of $\sim 2 \times 10^{-4}$.(FWHM) and a large solid angle acceptance that is three times larger than that of HRS. Its application is one of the important factors in achieving both high resolution and high yield in order to study spectroscopy of heavy hypernuclei. Its excellent detector system further cleanly identifies kaons.

One single target chamber will be used for all the planned targets including those to be used for calibrations. The entire system is vacuum connected.

Overall, this experimental design is for (1) the highest possible resolution (~600 keV FWHM in the case of thick solid targets), (2) the highest reachable yield, and (3) the lowest ever achievable background in electro-production of hypernuclei. Both involved spectrometers are well known and used previously with standard detector systems. The only new pieces of equipments are the Septum magnets and target system.

3.2 Kinematics

The proposed kinematics is based on the use of a beam energy of E = 4.5238 GeV, the minimum HRS angle available when using a Septum for an e' central momentum at ~3 GeV/*c*, and a maximized overlap of the virtual photon angular range to the HKS angular acceptance in order to obtain the highest possible production yield. The kinematics parameters and ranges are listed in Table 3-I. With this kinematics, both the spectrometers are located at sufficiently large angles with respect to the beam to avoid the forward scattered electrons and positrons. These were the sources of high accidental background in the previous Hall C hypernuclear experiments.

Table 3-I: Basic kinematics parameters of the Septum+HRS and Septum+HKS systems.

Beam energy (12 GeV mode, 2-passes, injector energy included)	4.5238 GeV
E' (HRS) central angle (horizontal and vertical bites)	7° (±1.5° and ±2.5°)
E' (HRS) central momentum (percentage bite)	3.0296 GeV/c (±4.0%)
Virtual photon central angle ($\phi=\pi$)	14°
Virtual photon energy range	1.37 – 1.62 GeV
Virtual photon momentum range	1.42 – 1.70 GeV/c
Average Q^2	-0.21 $(GeV/c)^2$
K^+ (HKS) central angle (horizontal and vertical bites)	14° (±4.5° and ±2.5°)
K^+ (HKS) central momentum (percentage bite)	1.2 GeV/c (±12.5%)

A GEANT simulation taking into account the realistic and known conditions of both the HRS and HKS was performed. No additional acceptance limitation was included for the new Septum magnets. Fig. 3-2 (a) shows the distribution of the Lab virtual photon angle θ_γ with the kinematics shown in Table 3-I. The shape of the distribution is due to the HRS momentum and angular acceptances. The virtual photons are aiming into the HKS angular acceptance in order to maximize the differential cross section and hence the production yield. Fig. 3-2 (b) shows the Q^2 range within the acceptance of the system.

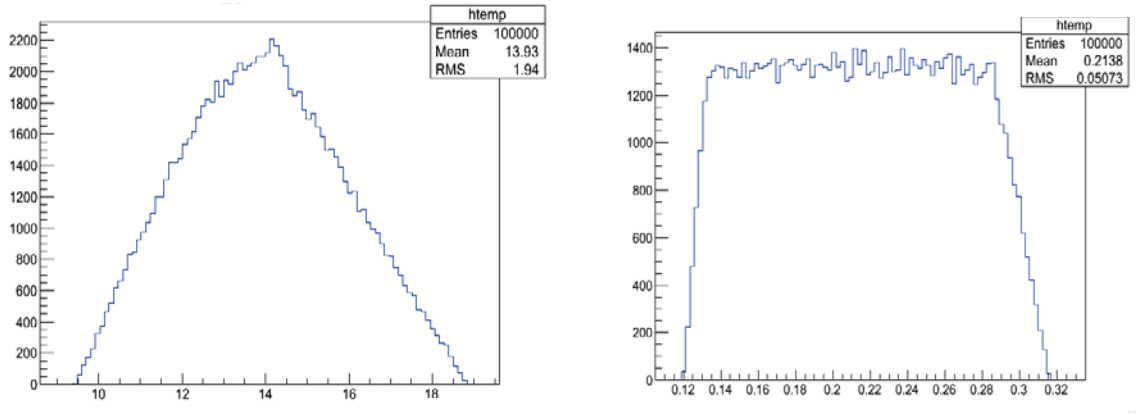

(a) $\theta_{e\gamma}$ Lab (Degrees) (b) Q^2 $(GeV/c)^2$

Figure 3-2: (a) Virtual photon angular distribution (symmetric with respect to $\phi = \pi$ plane defined by the central e and e' plane) in Lab system with respect to beam; (b) Q^2 acceptance.

Fig. 3-3 is an illustration of the e' and K^+ momentum correlation for various mass of hyperons (Λ and Σ^0) and ground state hypernuclei ($^{12}_{\Lambda}B$ and $^{208}_{\Lambda}Tl$). The broadening of Λ and Σ^0 is from the range of recoil angles. Free Λ and Σ^0 productions are important for calibration of the absolute missing mass scale.

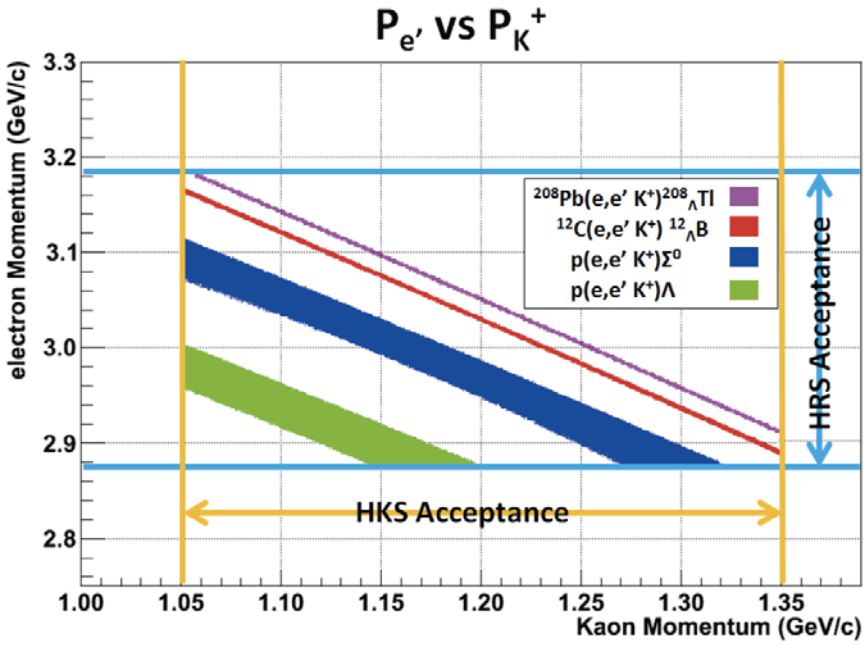

Figure 3-3: Mass correlation in the two dimensional momentum acceptances.

3.3 A draft design of the new Septum magnets

Fig. 3-4 shows the top view of the draft design of the two Septum magnets that will be used in conjunction with the HRS and HKS spectrometers. The kinematics and optics conditions of the two spectrometers were taken into account. Fig. 3-5 is a 3-D drawing showing the top half of the magnets and their coils. The post beam pipe passes through the half circular opening on the return yoke. This section of pipe uses magnetic field shielding material to minimize the influence from the fringe field on the exiting beam. Small correctors can be mounted behind the Septum to aim the beam correctly at the hall dump. Both the Septum technique and application of correctors were successfully used in the previous experiments.

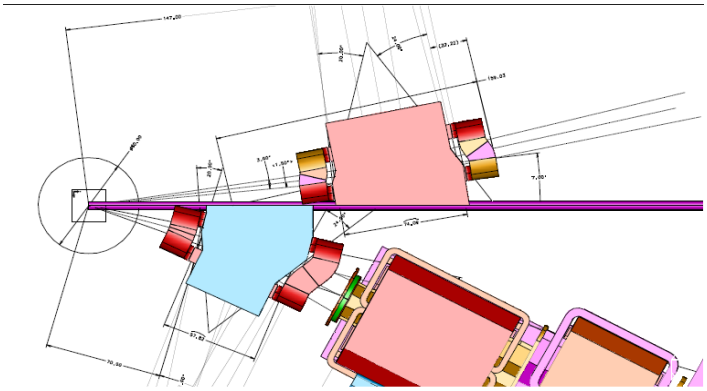

Figure 3-4: Illustration of the draft design of the two Septum magnets and their geometric relationship to the target chamber and subsequent spectrometers.

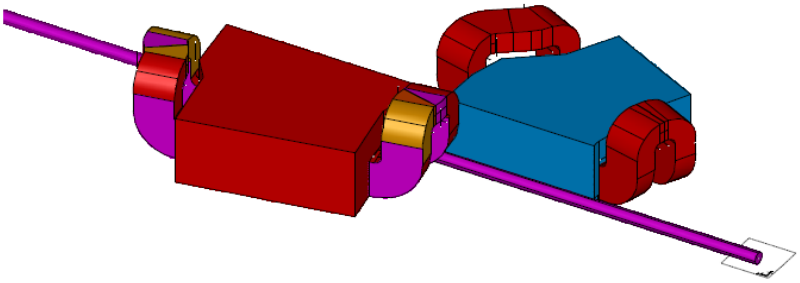

Figure 3-5: 3-D illustration of the two Septum magnets and the post beam pipe. Minimum influence of the fringe field to the post beam will be achieved by making the Septum "H" type and using magnetic shielding material for this section of pipe. Small correctors will be needed behind the Septum.

The major design parameters for consideration are listed in Table 3-II. The front distance is minimized to keep the HKS total path length as short as possible to maximize the K^+ survival rate. At the same time, sufficient space is maintained for the target chamber. A common sieve slit device may be mounted inside the target chamber where no fringe field from Septum is present. Introduction of the incline angles α and β is to reduce the horizontal dispersion and minimize the influence to the horizontal angular acceptance. The central and bend angles are driven by the conditions for separation of the forward scattered

particles, the required minimum space between the two spectrometers, and maximization of the yield. The field strength is chosen to be as low as possible to simplify the magnet design. The gaps are decided based on the vertical acceptance requirement from the HRS and HKS spectrometers.

Table 3-II: Basic design parameters of the Septum magnets for the HRS and HKS spectrometers.

Basic parameters	Septum (HRS)	Septum (HKS)
Front drift distance	147 cm	70 cm
Central angle	7°	14°
Horizontal angular bite	~±1.5°	~±4.5°
EFB incline angle α	-20°	-20°
EFB incline angle β	-24°	-24°
Bending angle ϕ	7°	12°
Field B	1.45 T	1.45 T
Rotation radius	707.49 cm	276.05 cm
Path length	86.44 cm	57.82 cm
Total integral Bdl	1.2534 T*m	0.8384 T*m
Gap	18 cm	12 cm

The target point will be determined by the Septum+HRS system. The Septum+HKS system is then located accordingly. The common target chamber has an outside dimension of 60-90 cm diameter. The target ladder contains both liquid/gas target cells and solid targets determined by the physics program and calibration needs. The ladder should be cooled to allow usage of the highest possible beam current. The chamber will have one incoming beam line connection port and exiting connection ports to the two spectrometers and the beam dump line. The sieve slit/collimator plates can be mounted on the target chamber and surveyed with respect to the target coordinates.

3.4 Yield rate comparison to the previous experiments

The new configuration of Septum+HRS/Septum+HKS aims to obtain almost background free spectroscopy for hypernuclei below the medium heavy mass region while maintaining good signal/accidental ratio for the heavy mass region.

The ground state peak of the $^{12}_{\Lambda}$B hypernucleus contains two states, $J^p = 1^-$ and 2^-. The combined photo-production cross-section with E_γ of about 1.5 GeV and θ_γ near zero is well known to be about 100 nb/sr in good agreement with both theory and (Hall A and C) experiments. Thus, the measured production yield of this peak by the Hall A and C experiments can be used to estimate the predicted yield with the new configuration. Table 3-III lists the gain factors over the previous Hall A and C experiments for various contributions, the combined total gain factor, and the estimated yield rate from known cross sections or production rates using the same luminosity. The results based on the previous experiments in Hall A and Hall C are consistent and their average is about 0.55 counts/hr/(1.0 nb/sr). A GEANT simulation using more precise information about the HKS and HRS predicted similar yield rates, 0.54 counts/hr/(1.0 nb/sr).

Table 3-III: Gain factor over the previous experiments and estimated production rate using the same luminosity.

Itemized gain factors by the new configuration	Over the previous Hall A experiment	Over the previous Hall C experiment
Integrated virtual photon flux ($\int\Gamma(E,E',\theta)dE'd\Omega$) per electron	2.16	0.91
K^+ survival rate	1.86	0.93
Integrated photo-production cross section ($\Delta\Omega_K$)	1.35	0.66
Beam current: 100μA	1	1
C target thickness: 100mg/cm^2	1	1
Total gain factor	5.42	0.56
Experimentally measured count rate (scaled to the same lum.)	10 counts/hr	100 counts/hr
Estimated count rate ($^{12}_{\Lambda}$B gs(1^- , 2^-), per 100nb/sr)	54 counts/hr	56 counts/hr

Although the yield rate is about half of the previous Hall C experiment which emphasized the yield, the production yield is still sufficiently high. The most important feature of the new configuration is the low accidental background. This is a significant difference from the previous Hall C experiments. In other words, the new configuration can be considered a significant upgrade of the Hall A experiment and increases its physics yield rate by a factor of five.

3.5 Spectrometer calibrations

Calibration of the spectrometer system is extremely important for the experiment to achieve its goal of high precision in determining the absolute mass (or Λ binding energy) and mass resolution. Standardized calibration methods and procedures successfully developed in the previous experiments will be applied again. A significant advantage of the new configuration is that these methods and procedures become more straight forward and can further improve the precision with much less analysis effort. This is because the two spectrometers are almost optically decoupled and there will be less information entanglement in the calibration data.

Some of light solid targets will be used for calibration as well as for precise determination of B_Λ. From experiences of previous hypernuclear programs at JLab, we learned that data for various solid targets with different energy loss contributions are quite useful to tune the backward matrix. We are considering using well studied CH_2, ^{10,11}B, ^{6,7}Li, ^{12}C targets for this purpose.

In addition to the above standard calibrations developed mainly for thin solid targets in the past, new calibrations will be needed for the extended target to further ensure excellent energy resolution. The major additional calibration is the reconstruction of the reaction ΔZ. A sequence of carbon foils at different Z will be used to collect data with known reaction Z position. ΔZ will be fit as a function of the 8 measured focal plane parameters from both spectrometers. For extended target, the ΔZ correction will be used in the momentum and reaction angle reconstructions.

A thin CH_2 target will be used as part of overall calibration. Simultaneous production of Λ and Σ^0 particles from CH_2 is important in calibrating the precise absolute mass scale.

3.6 Conclusion of this section

The configuration designed for the future hypernuclear physics experiments promotes high yield and clean spectroscopy. It makes possible the study of hypernuclei with high precision in a wide mass range (from few-body with extended targets to heavy systems with thin solid targets) at small Q^2 and a significant range of CM $\theta_{\gamma K}$ angles. As a flagship experiment of JLab hypernuclear programs, spectroscopy of $^{40}_{\Lambda}$K and $^{48}_{\Lambda}$K will be carried out as a first step with a new setup of HKS+HRS spectrometers which inherits advantages of previous hypernuclear experiments at JLab Hall-A and Hall-C.

4. Yield, resolution estimation and requested beamtime

The experiment will use solid targets. Detailed design of the targets will be optimized in collaboration with the JLab target group. The estimation was carried out with the well-established GEANT4 model for HKS and a newly modeled HRS with an index dipole magnetic field calculated by TOSCA (Fig.4-1).

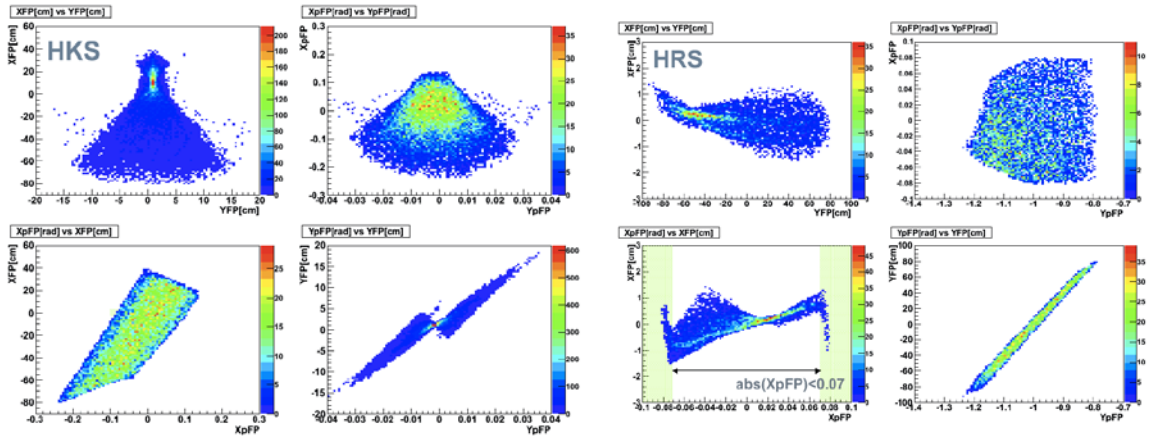

Figure 4-1: GEANT simulation results for HKS and HRS spectrometers. Focal plane parameters (positions at focal planes, XFP, YFP; angles at focal planes XpFP, YpFP) were calculated with GEANT models and results were compared with experimentally measured acceptances to check the varidity of models.

4.1 Expected mass resolution

The following factors contribute to the total mass resolution of the (e,e'K^+) experiment and they are summarized in Table 4-I.

1. Spectrometers' momentum resolution.

   Since HKS (K^+) and HRS (e') are already established spectrometers, relative momentum resolutions are known.

2. Beam energy resolution.

   We assumed $dE/E < 5 \times 10^{-5}$ for a 4.5 GeV electron beam.

3. Kinematic broadening due to uncertainty of the K^+ and e' scattering angles.

   The uncertainties of the K^+ and e' emission angles originate from multiple scattering through the materials between the target and tracking chambers in addition to the

angular resolution of the spectrometer itself. This effect is significant for hyperon elementary production or light hypernuclei, but less significant for heavier nuclei since the recoil of the hypernuclei is much smaller.

4. Energy loss and straggling in the target.

   Since our vertex resolution is not enough to determine the reaction point in the solid target (typically the thickness is less than a half mm while the gaseous target thickness is 200 mm), so energy loss of charged particles can be corrected only as an average. Its distribution including straggling will contribute the final mass resolution. For kaons, both the energy loss distribution due to the reaction point distribution and straggling will contribute while the sum of energy losses in the target for the beam and scattered electron is roughly constant and thus only straggling is problem. These effects were estimated with a GEANT simulation.

5. Uncertainty of the reaction point in the beam axis direction (ΔZ).

   As mentioned already, only the HRS has sensitivity to the reaction point in the Z direction, meaning that the HKS does not have it to first order since both the Septum and HKS are horizontal bending magnets. Uncertainty in Z does not make a problem for solid targets since their thickness is typically less than 0.5 mm, however, it affects the resolution for gaseous targets. Using a GEANT simulation, ΔZ resolution was estimated for the HRS and the reaction points in the simulation for the HKS were randomly distributed in ΔZ to estimate the deterioration of the HKS resolution. In the real analysis, the focal plane information of HRS and HKS can simultaneously be used to reach the best resolution.

Table 4-I: Estimation of mass resolution for ^{12}C and ^{40}Ca targets (unit is in keV).

Target	^{12}C (100 mg/cm^2)	^{40}Ca (100 mg/cm^2)
Beam	220	220
e' spectrometer	300	300
K spectrometer	220	220
K, e' angles	105	35
Energy loss/straggling	380	330
Total	590	550

4.2 Expected yield and required beam time

Using the estimated $^{12}_{\Lambda}B_{g.s.}$ yield rate in section 3.4, hypernuclear yields for various targets are summarized in Table 4-II.

It was assumed that the background originates from the accidental coincidence between K^+ and e' and the background spreads uniformly in the acceptance of the missing mass. The quasi-free production cross section of K^+ and e' are in proportion respectively to $A^{0.8}$ which was estimated from the $^{12}C(\gamma, K^+)$ reaction and A which is expected in DIS region. All solid targets' thicknesses are normalized to be 100 mg/cm^2 except for CH_2.

Necessary beam time was estimated to have enough events for major shell peak energies to be statistically determined with an accuracy of 50 keV. Signal to noise ratio is calculated with the numbers of signal in $\pm 1\sigma$ of Gaussian peak and background events under the peak.

Table 4-II: Yields estimation for various targets.

Target and objective hypernucleus	Beam current (μA)	Target thickness (mg/cm^2)	Assumed cross section (nb/sr)	Expected Yield (/hour)	Num. of events	Req. beamtime (hours)	B.G. Rate (/MeV/h)	S/N ($\pm 1\sigma$)	Comments
CH_2	2	500	200	19	1000	54	0.05	252	Calibration
^{6,7}Li	50	100	10	5.4	150	28	1.3	4.9	Calibration
^{9}Be	100	100	10	36	300	9	4.7	8.8	Calibration
^{10,11}B	25	100	10	16	150	19	0.29	33	Calibration
^{12}C	100	100	100	54	2000	37	4.4	17	Calibration
Subtotal for calibration targets						**147**			
^{40}Ca ($^{40}_{\Lambda}$K)	50	50	10	0.9	200	230	0.43	4.0	
^{48}Ca ($^{48}_{\Lambda}$K)	50	50	10	0.7	200	278	0.42	3.5	
Subtotal for heavier targets						**508**			
Total						**655**			

5. Summary

Based on more than a decade of experience at JLab, Hall A and Hall C, the JLab Hypernuclear Collaboration proposes the ^{40}Ca(e, e′ K^{+})$^{40}_{\Lambda}$K and ^{48}Ca(e, e′ K^{+})$^{48}_{\Lambda}$K experiment to investigate the isospin dependence of the hyperon-nucleon interaction and provide accurate and precise reference data for medium-to-heavy hypernuclear Λ separation energies.

The experiment will utilize well-established magnetic spectrometers HRS and HKS that were successfully used in the previous hypernuclear programs in Hall A and Hall C. Here, we summarize the important parameters and required resources for conducting of the experiment.

Key Experimental Parameters:

Beam energy: 12 GeV mode, 2-pass: 4.5238 GeV, Hall-A,
Requested beam time in total: 675 h = 28 days,
Range of beam currents: 2 to 100 μA,
Major apparatus: HKS, HRS, and Septa magnets.

Required resources: Major installations and new support structures:

HKS and Septa need major installation of magnets and detector packages,
HKS needs a new support for Hall A.

(New support structure for the Septa and Shielding houses for detectors are necessary.)

Major Equipment:

Magnets: HRS in Hall A, HKS (KQ1, KQ2 and KD), new Septum magnets (the 2nd can be the previously used super-conducting septum)

Power Supplies: HKS-D (252V, 1254A), HES-D (250V, 1100A) have own PS's provided by Tohoku University, all other PS's necessary are to be prepared by JLab.

Targets: Solid targets (CH_2, ^{6,7}Li, ^{9}Be, ^{10,11}B, ^{12}C, ^{40}Ca, ^{48}Ca)
Detectors: Standard detectors for HRS and HKS-detector package (Drift Chambers, TOF walls, Aerogel Chrenkov, Water Cherenkov.)

Electronics: Standard electronics, F1-TDCs, Amp-discriminator cards for drift chambers, FPGA based special trigger modules developed by Tohoku University (TUL-8040).

Computer Hardware: Standard

Possible Hazard

Electrical Equip.: high voltages for PMT, Drift Chambers, large currents for magnets

Flammable gas for drift chambers: Argon Ethane 50/50, 0.15 l/min each for HRS and HKS.

Targets: Condition 1, 2 are single spectrometer calibration with elastic scattering. Condition 3-7 are for calibration with coincidence measurement, 8-12 are for the physics run with gaseous cryogenic target and 13-15 with solid medium and heavy targets.

Condition #	Beam Energy (MeV)	Beam Current (μA)	Special Request	Target Material	Material Thickness (mg/cm^2)	Est. Beam on time (hours)
1	1200	10		Ta	100	10
2	3000	10		Ta	100	10
Single Arm. Calib						**20**
3	4523.8	2	2×2 mm^2 raster	CH_2	500	54
4	4523.8	50	2×2 mm^2 raster	$^{6,7}Li$	100	28
5	4523.8	100	No raster	^{9}Be	100	9
6	4523.8	25	2×2 mm^2 raster	$^{10,11}B$	100	19
7	4523.8	100	No raster	^{12}C	100	37
Subtotal calibration						**147**
13	4523.8	50		^{40}Ca	50	230
14	4523.8	50		^{48}Ca	50	278
Subtotal physics targets						**508**
Grand Total						**675**

Appendices

A. Electro-magnetic background in the kaon spectrometer

The HKS suffered from high rate backgrounds during the E05-115 runs. The source of background was carefully analyzed and a detailed GEANT4 simulation revealed the source of it.

The HKS with a Splitter magnet used in E05-115 was designed to avoid secondary e^+'s created in the target with its' optics. Such e^+ cannot reach the HKS detectors, however, some of them will hit the material just outside of the HKS dipole and create tertiary e^+ e^- pairs. Though such a probability is small, the large-Z target created lots of secondary e^+'s and then the tertiary e^+e^- background was not negligible.

Simulation with the GEANT4 model that includes vacuum extensions shows the source position of such background (Fig. A-1). The tracking information of real data proved that the majority of the background originated from a flange for a NMR port on the vacuum extension box.

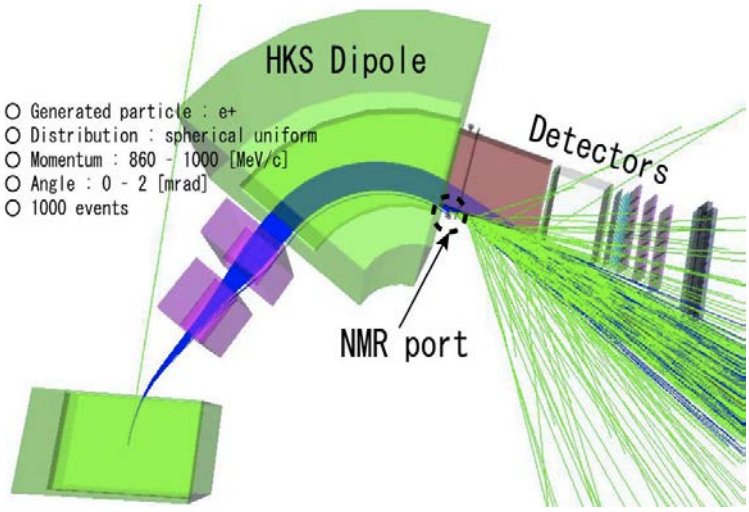

Figure A-1: GEANT4 simulation for electro-magnetic background experienced in the E05-115 experiment.

We modeled a septum magnet and combined it with the well-established HKS model in GEANT4. In the simulation of Septum + HKS, 10^{10} electrons were introduced in 100 mg/cm^2 Pb target and no secondary e^+'s reached the HKS exit.

It corresponds to 16 μs of 100 μA beam irradiation and thus background in the HKS originating from this source should be less than 62.5 kHz which does not cause any serious problem to the HKS detectors.

B. Theoretical predicted spectroscopy for selected hypernuclei

There are theoretical predictions on expected missing mass spectra to be obtained by the (e, ,e-′.K^+) reactions. This information was used in the design of the proposed experiment and will be further used in the detailed analysis to extract hypernuclear structure information.

B.2 ^{40}Ca(e,e'K$^+$)$^{40}_{\Lambda}$K reaction

The ^{40}Ca target is doubly *LS*-closed up to the $0d_{3/2}$ shell. As shown in Fig.B-2, the ^{40}Ca(γ,K^+)$^{40}_{\Lambda}$K excitation function calculated by DWIA with the SLA model [Byd12], the $^{40}_{\Lambda}$K's natural parity states (2^+,3^-,4^+) are expected to be populated predominantly. Therefore, we can extract $s^{\Lambda}_{1/2}$, $p^{\Lambda}_{3/2}$ and $d^{\Lambda}_{5/2}$ energies from these peaks with less ambiguity. We can expect major shell peaks (Λ in s, p, d, f waves) with the production cross section of 100 nb/sr and core excited states with 10-100 nb/sr.

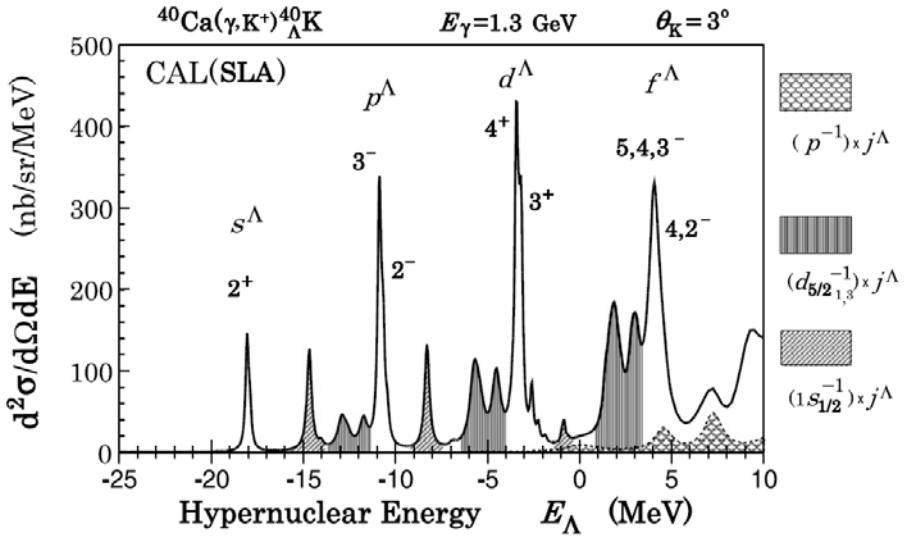

Figure B-2: Calculated ^{40}Ca(γ,K^+)$^{40}_{\Lambda}$K excitation function by DWIA with SLA model. The calculation assumed E_γ = 1.3 GeV, $\theta_{\gamma K}$ = 3° and function *ls*-splitting of 0.17(2*l* +1) MeV [BYD12].

[BYD12] P. Bydžovský and D. Skoupil, **arXiv:1212.0337v1** [nucl-th].